
Article:
Astier, S., Johnson, E.C. orcid.org/0000-0002-0092-1008, Norvilaite, O. et al. (5 more authors) (2024) Controlling adsorption of diblock copolymer nanoparticles onto an aldehyde-functionalized hydrophilic polymer brush via pH modulation. Langmuir, 40 (7). pp. 3667-3676. ISSN 0743-7463

https://doi.org/10.1021/acs.langmuir.3c03392

LANGMUIR

pubs.acs.org/Langmuir Article

Controlling Adsorption of Diblock Copolymer Nanoparticles onto an Aldehyde-Functionalized Hydrophilic Polymer Brush via pH Modulation

Published as part of Langmuir virtual special issue "Highlights in Interface Science and Engineering: Polymer Brushes".

Samuel Astier, Edwin C. Johnson,* Oleta Norvilaite, Spyridon Varlas, Emma E. Brotherton, George Sanderson, Graham J. Leggett, and Steven P. Armes*

Cite This: *Langmuir* 2024, 40, 3667−3676 Read Online

ABSTRACT: Sterically stabilized diblock copolymer nanoparticles with a well-defined spherical morphology and tunable diameter were prepared by RAFT aqueous emulsion polymerization of benzyl methacrylate at 70 °C. The steric stabilizer precursor used for these syntheses contained pendent *cis*-diol groups, which means that such nanoparticles can react with a suitable aldehyde-functional surface via acetal bond formation. This principle is examined herein by growing an aldehyde-functionalized polymer brush from a planar silicon wafer and studying the extent of nanoparticle adsorption onto this model substrate from aqueous solution at 25 °C using a quartz crystal microbalance (QCM). The adsorbed amount, Γ, depends on both the nanoparticle diameter and the solution pH, with minimal adsorption observed at pH 7 or 10 and substantial adsorption achieved at pH 4. Variable-temperature QCM studies provide strong evidence for chemical adsorption, while scanning electron microscopy images recorded for the nanoparticle-coated brush surface after drying indicate mean surface coverages of up to 62%. This fundamental study extends our understanding of the chemical adsorption of nanoparticles on soft substrates.

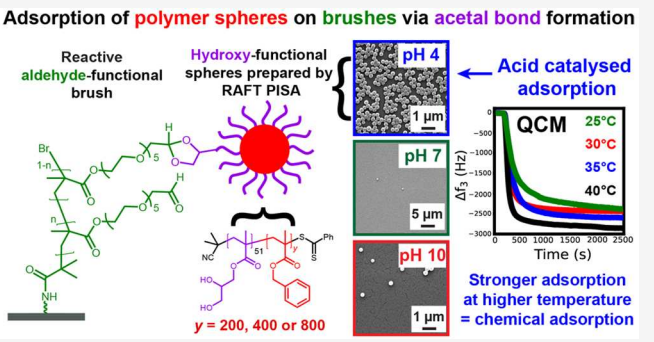

INTRODUCTION

Understanding and controlling particle adsorption at interfaces is fundamental to commercial products such as paints[1] and coatings,[2,3] as well as for the preparation of colloidosomes,[4] Pickering emulsions,[5] liquid marbles,[6−9] and long-lived foams.[10] In principle, such adsorption may involve physical interactions such as electrostatic attraction, hydrogen bonding, van der Waals forces, or the formation of new bonds (i.e., chemical adsorption).

The quartz crystal microbalance (QCM) is a well-established analytical technique in surface science. It is extremely sensitive to changes in mass, *m*, owing to adsorbed species because this causes a reduction in the frequency of an oscillating quartz crystal, Δ*f*, which can be determined with high precision. Sauerbrey derived a simple relationship, which has become widely known as the Sauerbrey equation (eq 1).

$$m = C \times \frac{\Delta f}{n} \quad (1)$$

Here *C* is a sensitivity constant (expressed in units of mg m^{-2} Hz^{-1}) and *n* is the overtone number.

Accordingly, QCM has been used to monitor the adsorption of a range of colloidal particles onto various model planar substrates, including gold,[11] silica,[12] cellulose,[13] and stainless steel.[14,15] Literature examples include the electrostatic adsorption of anionic silica nanoparticles onto a modified cationic substrate,[16] the adsorption of gold nanoparticles for the design of biosensors,[17−20] and the adsorption of charged diblock copolymer micelles onto oppositely charged surfaces.[21−26] Under appropriate conditions, QCM-D (where D denotes dissipation) can also be employed to reveal structural information regarding the nature of the adsorbed material.[27,28]

Received: November 6, 2023
Revised: January 12, 2024
Accepted: January 15, 2024
Published: February 6, 2024

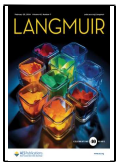

https://doi.org/10.1021/acs.langmuir.3c03392
Langmuir 2024, 40, 3667−3676

However, most of these prior studies (i) have focused on physical adsorption rather than chemical adsorption and (ii) involve relatively hard (as opposed to soft[29]) substrates.

Over the past decade or so, polymerization-induced self-assembly (PISA) has become widely recognized as a powerful platform technology for the rational synthesis of a wide range of block copolymer nanoparticles.[30−38] PISA involves the chain extension of a soluble block A in a suitable solvent using a monomer that forms an insoluble block B. Accordingly, in situ self-assembly occurs at some critical degree of polymerization (DP) for the second block to produce sterically stabilized nanoparticles, whereby the B block is located within the cores and the A block confers steric stabilization.[39,40] Various research groups have developed highly efficient one-pot syntheses for many PISA formulations.[41−43] Moreover, PISA can be conducted using a wide range of solvents (including either water or oil) and the overall particle diameter can be systematically varied over a wide range in the case of kinetically trapped spheres.[26,44−51] This enables the convenient synthesis of libraries of sterically stabilized nanoparticles for model studies simply by adjusting the target DP for the insoluble core-forming block.[52−54]

For example, introducing epoxy groups into hydrophobic nanoparticles leads to their much stronger adsorption from mineral oil onto stainless steel.[15] Enhanced adsorption from aqueous solution onto the same planar substrate was also achieved for suitably modified hydrophilic nanoparticles.[14] PISA has also proved to be useful for establishing the essential design rules for nanoparticle occlusion within calcite crystals[55,56] and for new nanoparticle dispersants to produce concentrated aqueous suspensions of micron-sized azoxystrobin crystals (a widely used broad-spectrum fungicide).[57,58]

Very recently, we demonstrated that nanoparticle interactions with a hydrophilic polymer brush can be mediated by dynamic covalent chemistry.[59] More specifically, aldehyde-decorated nanoparticles can adsorb strongly onto a primary amine-functionalized brush via Schiff base chemistry (i.e., the formation of multiple imine bonds). Herein we report that an aqueous PISA formulation can be used to prepare *cis*-diol-functionalized spherical nanoparticles of tunable size. The effect of varying the solution pH on the extent of adsorption of such nanoparticles onto a hydrophilic aldehyde-functional planar brush is monitored using a QCM and scanning electron microscopy (SEM). Overall, our experimental data provide strong evidence for the formation of acetal bonds, rather than merely physical adsorption.

EXPERIMENTAL SECTION

Materials. Unless stated otherwise, all of the reagents were used as received. Glycerol monomethacrylate (GMA) and the *cis*-diol-capped oligo(ethylene glycol) monomethacrylate (GEO5MA) monomer were donated by GEO Specialty Chemicals (Hythe, UK) and used without further purification. Benzyl methacrylate (BzMA), 4,4′-azobis(4-cyanopentanoic acid) (ACVA; 99%), (3-aminopropyl)-triethoxysilane (APTES; 99%), 2-bromoisobutyryl bromide (BiBB; 98%), sodium periodate ($NaIO_4$; > 99%), and dichloromethane (DCM; > 99%) were purchased from Sigma-Aldrich (UK). 2-Cyano-2-propyldithiobenzoate (CPDB) was purchased from STREM Chemicals Ltd. (Cambridge, UK). *N*,*N*,*N*′,*N*″,*N*″-Pentamethyldiethylenetriamine (PMDETA; 98%), tetrahydrofuran (THF), ethanol, dimethylformamide (DMF), and hydrochloric acid (HCl, 37%) were purchased from Fisher Scientific (UK). Sodium hydroxide pellets (NaOH, 98%) were purchased from Alfa Aesar. Copper(II) chloride ($CuCl_2$; 99%) was purchased from Acros Organics (UK). Deuterated dimethylformamide (d_7-DMF) was purchased from Goss Scientific Instruments Ltd. (Cheshire, UK). Test-grade silicon wafers (100) were purchased from PI-KEM (Tamworth, UK). Deionized water was used for all experiments involving aqueous solutions.

Characterization Techniques. *^{1}H NMR Spectroscopy.* Spectra were recorded in d_7-DMF using a 400 MHz Bruker AVANCE-400 spectrometer at 298 K with 16 scans being averaged per spectrum.

Aqueous Electrophoresis. Zeta potentials for diblock copolymer nanoparticles were analyzed using a Malvern Zetasizer Nano ZS instrument equipped with a 4 mW He−Ne laser (λ = 633 nm) operating at a fixed scattering angle of 173°. Samples were diluted to 1% w/w using 1 mM KCl, with either dilute NaOH or HCl being used for pH adjustment as required. Zeta potentials were calculated from the Henry equation using the Smoluchowski approximation.

DMF Gel Permeation Chromatography. DMF gel permeation chromatography (GPC) was used to assess the molecular weight distribution of each (co)polymer. The instrument setup comprised two Agilent PL gel 5 μm Mixed-C columns and a guard column connected in series to an Agilent 1260 Infinity GPC system operating at 60 °C. The GPC eluent was high-performance liquid chromatography-grade DMF containing 10 mM LiBr at a flow rate of 1.0 mL min^{-1}, the copolymer concentration was typically 1.0% w/w, and calibration was achieved using a series of ten near-monodisperse poly(methyl methacrylate) (PMMA) standards ranging from 1080 to 905,000 g mol^{-1}. Chromatograms were analyzed using Agilent GPC/SEC software.

Dynamic Light Scattering. Dynamic light scattering (DLS) studies were performed using a Malvern Zetasizer Nano-ZS instrument equipped with a 4 mW He−Ne laser (λ = 633 nm) operating at a fixed scattering angle of 173°. Copolymer dispersions were diluted to 0.1% (w/w) using deionized water prior to light scattering studies at 25 °C, with 2 min being allowed for thermal equilibrium prior to each measurement. The hydrodynamic z-average particle diameter was calculated via the Stokes−Einstein equation.

Spectroscopic Ellipsometry. Measurements were performed in air at 20 °C on bare planar silicon wafers, initiator-functionalized silicon wafers, and polymer brush-functionalized silicon wafers using a J. A. Woollam M2000 V ellipsometer at a fixed angle of incidence of 75° normal to the sample surface. A wavelength range of 370−1000 nm was used to obtain two ellipsometry parameters (Ψ and Δ). Data analysis and modeling were performed using Woollam CompleteEASE software. The Ψ and Δ values were fitted using a two-layer model comprising a native oxide layer and a Cauchy layer to describe the polymer brush. Cauchy parameters were A_n = 1.482, B_n = 0.0056 μm^{-2}, and C_n = 0. The ellipsometer setup allowed a relatively large area (approximately 0.5 × 1 cm) to be sampled; this corresponds to around 30% of the total area of each brush sample.

Transmission Electron Microscopy. Copper/palladium transmission electron microscopy (TEM) grids (Agar Scientific, UK) were coated in-house with a thin film of amorphous carbon. Grids were then subjected to a glow discharge for 30 s to create a hydrophilic surface. Each 0.1% w/w aqueous diblock copolymer dispersion was deposited as a 5.0 μL droplet onto a freshly treated grid for 1 min and then blotted with filter paper to remove excess solution. To stain the deposited nanoparticles, uranyl formate (5.0 μL of a 0.75% w/w aqueous solution) was placed on the sample-loaded grid for 20 s and then carefully blotted to remove excess stain. Each grid was then dried using a vacuum hose. Imaging was performed using a FEI Tecnai Spirit 2 instrument operating at 80 kV and equipped with an Orius SC1000B camera.

Quartz Crystal Microbalance. QCM sensors coated with a 50 nm silica overlayer (QSX 303, ∼ 5 MHz fundamental frequency) were purchased from Q-Sense (Sweden). Each sensor was cleaned according to the manufacturer's instructions. This protocol involved (i) UV/O_3 treatment for 15 min (BioForce UV/O_3 cleaner, ∼ 9 mW cm^{-2}, λ = 254 nm), (ii) exposure to 2% w/w sodium dodecyl sulfate solution for 30 min, (iii) copious rinsing with deionized water and drying under N_2, and (iv) a final UV/O_3 treatment for 15 min. The resulting substrates were functionalized with the ATRP initiator prior

https://doi.org/10.1021/acs.langmuir.3c03392
Langmuir 2024, 40, 3667−3676

Scheme 1. Synthesis of $PGMA_{51}$−$PBzMA_x$ Diblock Copolymer Nanoparticles via RAFT Aqueous Emulsion Polymerization of BzMA to Afford Spherical Nanoparticles. Increasing the Target DP of the PBzMA Block (y) Leads to a Systematic Increase in the Mean Nanoparticle Diameter

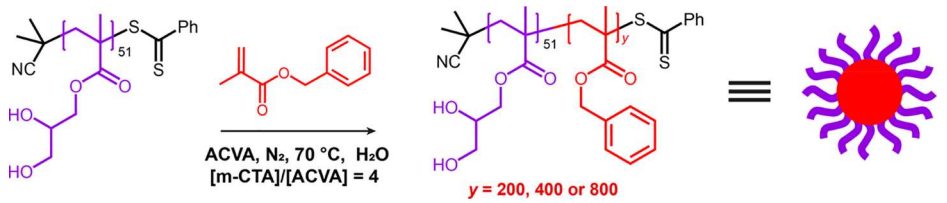

to surface-initiated polymerization to produce brush-coated substrates using the protocols given below.

QCM measurements were performed using an openQCM NEXT instrument (Novaetech S.r.l., Italy) equipped with a temperature-controlled cell connected to a Masterflex Digital Miniflex peristaltic pump (Cole-Parmer Instrument Company, UK). A rapid flow of ethanol (2 mL min^{-1}) was used to wet the inner cell surface. Once all bubbles had been removed, water (either pH 4, 7, or 10) was flowed through the cell until the sensor frequency exhibited a drift of less than 1 Hz min^{-1}. This typically occurred within 1 h of filling the cell. Once a stable signal was obtained, a 1% w/w aqueous dispersion of nanoparticles at the desired solution pH was passed through the cell at a flow rate of 0.1 mL min^{-1} (minimum flow volume = 3 mL). Once any signal drift had abated, water at the same pH was passed through the cell at the same flow rate, and the experiment was terminated after returning to minimal signal drift. Most QCM experiments were performed at 25 °C but some measurements were also conducted at 30, 35, or 40 °C.

The adsorbed amount can be calculated using various models. The simplest and most widely applied model uses the Sauerbrey equation, which relates the change in frequency, Δf, to the change in adsorbed mass per unit area, m.

$$m = C \times \frac{\Delta f}{n}$$

where C is a sensitivity constant −0.177 mg m^{-2} Hz^{-1}, Δf is the change in resonant frequency (Hz), and n is the overtone number. The third harmonic (n = 3) was used to calculate the adsorbed amount to avoid experimental artifacts associated with the fundamental harmonic. The Sauerbrey equation has been shown to be applicable when the $\Delta D_n/\Delta f_n$ ratio is greater than 0.1×10^{-7} Hz^{-1}.[60,61] All adsorbed masses presented herein are validated using this ratio.

Scanning Electron Microscopy. Scanning electron microscopy (SEM) images were acquired using an FEI Inspect F field emission scanning electron microscope operating at an acceleration voltage of 10−20 kV. All samples were prepared by drying dilute aqueous nanoparticle dispersions (0.1% w/w) onto silicon wafers at 25 °C. The sample-loaded silicon wafers were mounted on aluminum stubs using adhesive carbon tabs. Silver paint was applied to two edges of the mounted silicon wafers before sputter-coating with a gold overlayer to prevent charge build-up. Surface coverages (%) for the adsorbed nanoparticles were assessed using *ImageJ* software and were averaged across multiple images recorded for each sample.

Synthesis Protocols. *Preparation of the $PGMA_{51}$ Precursor.* GMA (78.144 g, 488 mmol), CPDB RAFT agent (1.9630 g, 8.873 mmol; target DP = 55), and ACVA (0.4970 g, 1.774 mmol; CPDB/ACVA molar ratio = 5.0) were weighed into a 500 mL round-bottom flask and degassed with a stream of nitrogen gas for 15 min. Ethanol (148 mL) was deoxygenated separately with nitrogen for 30 min prior to its addition to the other reagents. The reaction solution was stirred and degassed in an ice bath for a further 30 min before placing in an oil bath set at 70 °C. The polymerization was allowed to proceed for 150 min, resulting in a GMA conversion of 68% as judged by ^{1}H NMR spectroscopy. The crude homopolymer was purified by precipitation into a ten-fold excess of DCM from methanol. This purification process was repeated twice to give a purified PGMA precursor (53.14 g, <1% residual GMA monomer; see Figure S1). Its mean DP was calculated to be 51 by end-group analysis using ^{1}H NMR spectroscopy. DMF GPC analysis indicated an M_n of 13,200 g mol^{-1} and an M_w/M_n of 1.23 (vs a series of near-monodisperse PMMA calibration standards).

RAFT Aqueous Emulsion Polymerization of Benzyl Methacrylate. A typical protocol for the synthesis of $PGMA_{51}$−$PBzMA_{200}$ diblock copolymer nanoparticles was conducted as follows: $PGMA_{51}$ precursor (0.30 g, 35.76 μmol), BzMA (1.28 g, 7.273 mmol), ACVA (2.5 mg, 8.939 μmol; CTA/ACVA molar ratio = 4.0), and water (14.3 g, targeting 10% w/w solids) were weighed into a 50 mL round-bottom flask and purged with nitrogen for 30 min at 20 °C. Then the flask was immersed in an oil bath set at 70 °C for 24 h. The reaction mixture was stirred with the aid of a magnetic flea, and the resulting diblock copolymer was analyzed by DMF GPC (M_n = 27,400 g mol^{-1}, M_w/M_n = 1.35 vs PMMA standards). ^{1}H NMR spectroscopy analysis of a freeze-dried sample dissolved in DMSO-d_6 indicated less than 1% residual BzMA monomer. DLS studies of a 0.20% (w/w) copolymer dispersion indicated an intensity-average particle diameter of 64 nm (DLS polydispersity, PDI = 0.07).

Silicon Wafer Cleaning. Silicon (100) wafers were cut into small pieces (~1 × 2 cm) before being cleaned by UV−ozone treatment for 60 min at 103 Pa using a BioForce Nanosciences ProCleaner. Wafers were then immersed in 2 M NaOH solution for 30 s, rinsed with Milli-Q water, and dried under compressed air prior to further UV−ozone treatment for 30 min.

Preparation of Initiator-Functionalized Silicon Wafers and QCM Sensors. Cleaned wafers and/or QCM sensors were placed in a Petri dish with a vial containing ~400 μL of APTES within a desiccator. A vacuum of 5 mbar was achieved within 5 min. Then the tap was closed, and the wafers were maintained under vacuum for 30 min at 20 °C. Substrates were then annealed in air for 30 min at either 110 °C (wafers) or 70 °C (QCM sensors).

After cooling to 20 °C, these APTES-modified substrates were immersed in anhydrous DCM before triethylamine and BiBB were sequentially added to the solution. The final concentrations of triethylamine and BiBB were both 0.2 mM (triethylamine/BiBB molar ratio = 1:1). The surface was reacted for 60 min. Each wafer or QCM substrates were then rinsed with ethanol and Milli-Q water before being dried under a stream of compressed air.

PGEO5MA Brush Growth via SI-ARGET ATRP. PGEO5MA brushes were grown from initiator-functionalized silicon wafers and QCM sensors using a previously reported protocol.[62] A polymerization mixture containing a 45% v/v aqueous solution of GEO5MA monomer, $CuCl_2$ catalyst, and PMDETA ligand was prepared in deionized water at a molar ratio of 1000:1:10. Ascorbic acid (ascorbic acid/$CuCl_2$ molar ratio = 4.0) was then dissolved in this aqueous mixture, which was stirred for 5 min at 20 °C. Either initiator-functionalized wafers and/or QCM sensors were immersed in this reaction solution, and the surface polymerization was allowed to proceed for 1 h. Substrates were removed and rinsed with copious amounts of ethanol and deionized water to quench the polymerization and then dried under a stream of compressed air.

Oxidation of a PGEO5MA Brush to Produce a PAGEO5MA Brush. As previously reported,[59,62] wafers and/or QCM sensors were immersed in a 3.0 g dm^{-3} aqueous solution of $NaIO_4$ for 30 min at

https://doi.org/10.1021/acs.langmuir.3c03392
Langmuir 2024, 40, 3667−3676

20 °C, washed extensively with ethanol and water, and then dried under a stream of compressed air.

Adsorption of $PGMA_{51}$−$PBzMA_{200}$ Nanoparticles onto a PAGEO5MA Brush. An aqueous dispersion of $PGMA_{51}$−$PBzMA_{200}$ nanoparticles was diluted to 1.0% w/w (~3 mL) with water and adjusted to pH 4, 7, or 10 using dilute HCl or NaOH as required. Brush-functionalized wafers (or bare silicon wafers in control experiments) were then immersed in these aqueous dispersions. Nanoparticle adsorption was allowed to proceed for 18 h at 22 °C prior to thorough rinsing with water (10 mL, at the same solution pH as that of the nanoparticle dispersion) and drying under a stream of compressed air.

RESULTS AND DISCUSSION

A series of $PGMA_{51}$−$PBzMA_y$ diblock copolymer nanoparticles (y = 200, 400 or 800) were prepared via RAFT aqueous emulsion polymerization of BzMA using a $PGMA_{51}$ precursor (Figure S1), as shown in Scheme 1. The PGMA steric stabilizer chains bear *cis*-diol functionality, which was exploited by Cunningham et al. to modulate their surface adsorption onto a patterned planar surface via dynamic covalent chemistry.[52] In the PISA literature, it is well-established that increasing the target DP of the core-forming block for a given steric stabilizer DP leads to a systematic increase in nanoparticle diameter.[46,63−67] ^{1}H NMR studies revealed that almost complete BzMA conversion (>99% conversion) was achieved within 24 h (Figure S2) while GPC analysis indicated efficient chain extension in each case (Figure S3), confirming the synthesis of well-defined diblock copolymers.

DLS studies indicated that the z-average diameter of the nanoparticles scaled proportionally with that of the target PBzMA DP (Figure 1a). TEM analysis confirmed a well-defined spherical morphology for each of the $PGMA_{51}$−$PBzMA_y$ nanoparticles, see Figure 1b−d. TEM and DLS particle size data are summarized in Table S1. It is perhaps worth mentioning that the PBzMA DPs targeted in this study were selected to ensure that the nanoparticles were sufficiently large to be readily discernible by SEM (see below).

Aqueous electrophoresis measurements (Figure S4) indicated that the nanoparticles were essentially neutral from pH 4 to pH 8 (zeta potentials ranged from −1 to −5 mV). Weakly anionic character was observed at pH 9−10 (zeta potential ~ −10 mV). This is most likely the result of using an ACVA initiator for the synthesis of the PGMA precursor. For RAFT polymerization, it is well-known that a minor fraction of chains become capped with initiator fragments, rather than the R group originating from the RAFT agent.[68] In the case of ACVA, this introduces a small number of carboxylic acid groups, which would account for the weakly anionic character observed at higher pH. One reviewer of this article has suggested that partial hydrolysis of the PGMA steric stabilizer chains might occur during the aqueous electrophoresis measurements. Such a side reaction would introduce methacrylic acid residues, which could contribute to the weakly negative zeta potentials indicated in Figure S4.

PGEO5MA brushes were prepared using our previously reported SI-ARGET ATRP protocol (Scheme 2).[62] Spectroscopic ellipsometry was used to determine dry brush thicknesses (~35 nm within 60 min of surface polymerization), with smooth brush surfaces and satisfactory data fits being achieved in each case. Each PGEO5MA brush was then oxidized using a 3.0 g dm^{-3} aqueous solution of $NaIO_4$. Subsequent ellipsometry studies of the dried brush revealed an

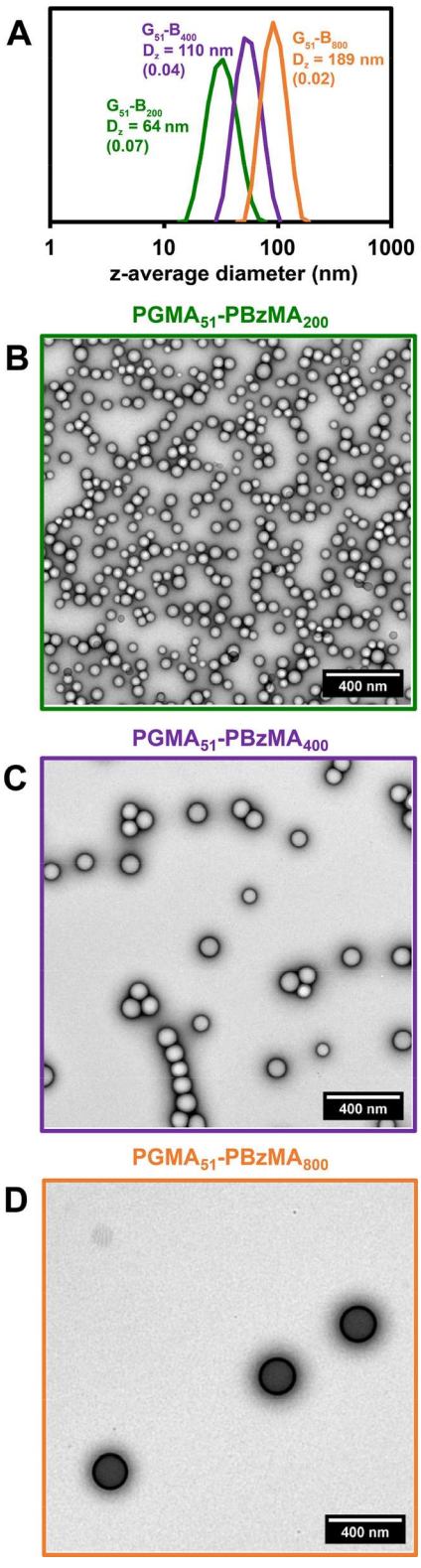

Figure 1. $PGMA_{51}$−$PBzMA_y$ diblock copolymer nanoparticles (y = 200, 400 or 800) prepared via RAFT aqueous emulsion polymerization of BzMA at 70 °C: (a) DLS particle size distributions (where "G" denotes PGMA and "B" denotes PBzMA) and (b−d) representative TEM images recorded for the three types of nanoparticles, illustrating their well-defined spherical morphology.

https://doi.org/10.1021/acs.langmuir.3c03392
Langmuir 2024, 40, 3667−3676

Scheme 2. Growth of a PGEO5MA Brush from a Planar Silicon Wafer via SI-ARGET ATRP Followed by Selective Oxidation of the Pendent *cis*-Diol Groups with $NaIO_4$ to Produce an Aldehyde-Functionalized PAGEO5MA Brush. Schematic Representation of the Attempted Adsorption of $PGMA_{51}$−$PBzMA_y$ Nanoparticles (y = 200, 400 or 800; See Scheme 1) onto the Aldehyde-Functionalized Brush via Acetal Bond Formation

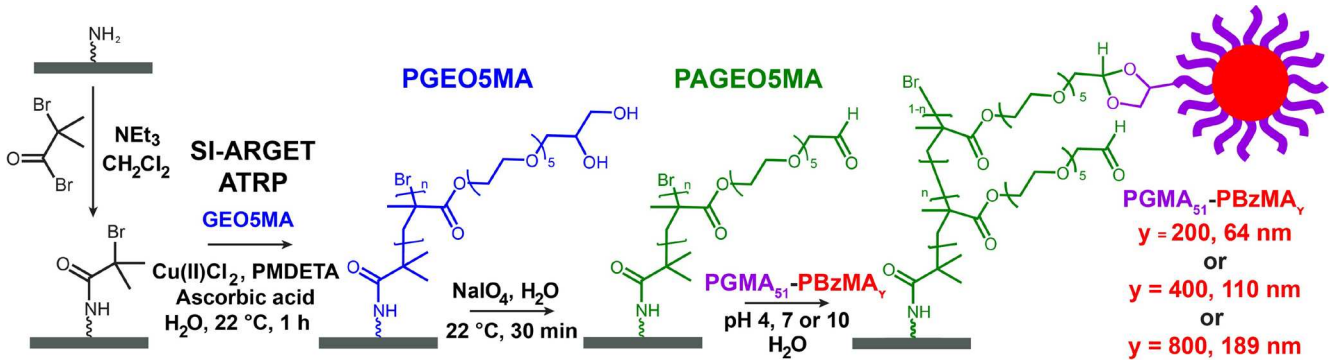

approximate 7% reduction in the dry brush thickness: this is consistent with the lower repeat unit mass expected after the loss of formaldehyde associated with selective oxidation.[62,69]

Non-ionic and zwitterionic hydrophilic polymer brushes are well-known for their ability to minimize biofouling.[70,71] On close approach to a well-solvated brush, proteins (and other biomacromolecules) typically experience a strong repulsive interaction owing to an increase in osmotic pressure.[72,73] The magnitude of this force depends on the inter-separation distance, brush grafting density,[72] and particle size,[74,75] as well as the precise geometry.[76]

If nanoparticle adsorption is desired, then an attractive interaction force between the brush and the nanoparticles must be introduced to overcome the repulsive force. Recently, we exploited dynamic covalent chemistry (more specifically, imine bond formation) to adsorb aldehyde-functional nanoparticles onto amine-functional polymer brushes.[59] Herein we examine whether the formation of acetal bonds between *cis*-diol-functional $PGMA_{51}$−$PBzMA_y$ nanoparticles and a hydrophilic aldehyde-functional polymer brush is sufficient to promote adsorption. It is well-known that acetal bond formation is (i) acid-catalyzed and (ii) more entropically favorable when using a diol rather than two separate alcohols.[77] The general reaction for acetal bond formation between an aldehyde and a *cis*-diol compound is shown in Scheme 3.

Scheme 3. Acid-Catalyzed Acetal Bond Formation When Reacting an Aldehyde with a *cis*-Diol Compound

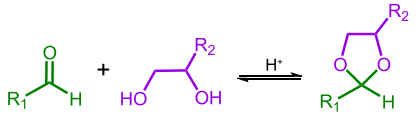

PAGEO5MA brushes were immersed in aqueous dispersions containing the three different types of nanoparticles at pH 4, 7, or 10, followed by rinsing with copious amounts of water at the same pH. The extent of nanoparticle adsorption was assessed by SEM (Figure 2). Clearly, extensive nanoparticle adsorption occurs at pH 4, with surface coverages (estimated by digital image analysis using *ImageJ* software) ranging from 50 to 61%. The apparent clustering at these very high surface coverages has been observed previously for similar nanoparticles adsorbed at planar interfaces.[14,38] In striking contrast, nanoparticle adsorption is much weaker at both pH 7 and pH 10 (surface coverage < 1−2% in each case). A summary of the surface coverage data is provided in Table S2. The remarkable enhancement in nanoparticle adsorption observed under mildly acidic conditions illustrates the importance of pH modulation in facilitating acetal bond formation. Moreover, these observations are consistent with prior small-molecule studies.[78]

QCM is widely used for the construction of various types of biosensors[17−20] and can also be used to characterize the viscoelastic properties of thin polymer films such as polymer brushes.[79−82] We have recently employed QCM to quantify the extent of adsorption of either diblock copolymer nanoparticles or nanosized oil droplets onto model soft substrates[14,15,83] and for the conjugation of a globular protein to a PAGEO5MA brush via Schiff base chemistry.[62] Herein we employ QCM to quantify the adsorption of $PGMA_{51}$−$PBzMA_y$ nanoparticles (y = 200, 400, or 800) onto PAGEO5MA brushes by determining the adsorbed mass per unit area (Γ, mg m^{-2}).[84,85]

With QCM, we first demonstrate that the aldehyde groups within the hydrophilic brush chains are essential for strong nanoparticle adsorption. PGEO5MA and PAGEO5MA brushes were grown from separate QCM sensors before being exposed in turn to the same 1.0% w/w dispersion of $PGMA_{51}$−$PBzMA_{800}$ nanoparticles at pH 4. A dramatic reduction in frequency was observed for the aldehyde-functional brush, which indicates strong nanoparticle adsorption at 25 °C; see Figure 3. Importantly, the change in frequency remains constant after rinsing with water at pH 4, indicating irreversible nanoparticle adsorption. In contrast, only a moderate reduction in frequency was observed for the hydroxy-functional PGEO5MA brush at the same temperature. Moreover, this frequency returns to close to its original value after rinsing with water at pH 4, indicating that most of the initially adsorbed nanoparticles are only weakly bound and can be readily washed off the brush surface. These findings are corroborated by the SEM images shown in Figure 3.

The adsorbed amount, Γ, calculated from the QCM data for nanoparticle adsorption on both types of brushes is indicated within Figure 3. The striking difference in the extent of adsorption for *cis*-diol-functional polymer nanoparticles on the *cis*-diol- and aldehyde-functional polymer brushes underlines the importance of acetal bond formation in promoting nanoparticle adsorption. In a separate control experiment, SEM studies confirmed that nanoparticle adsorption onto a

https://doi.org/10.1021/acs.langmuir.3c03392
Langmuir 2024, 40, 3667−3676

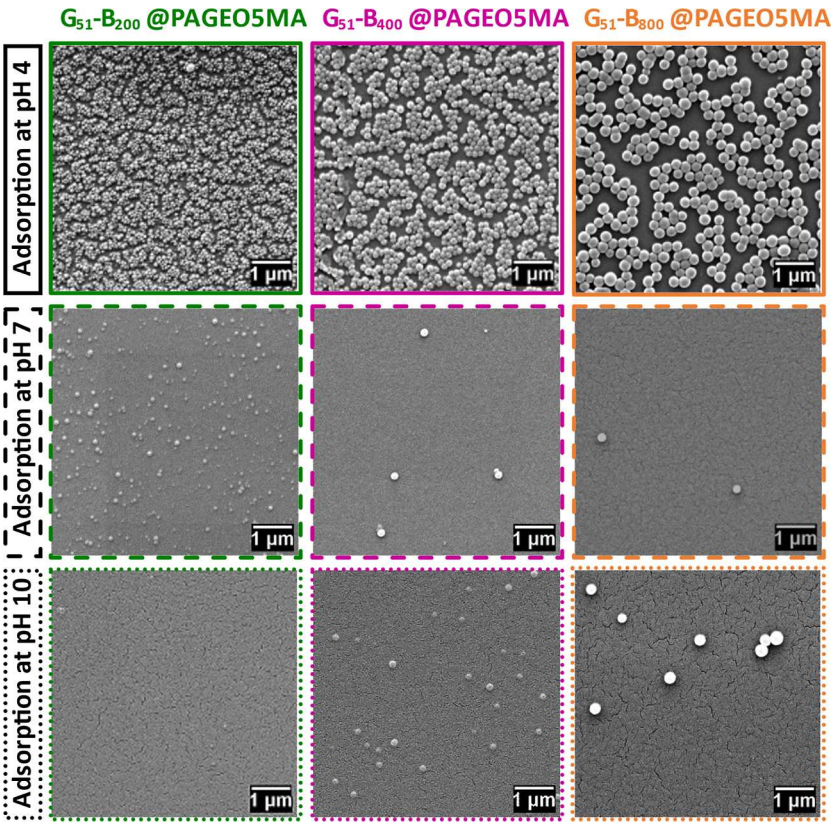

Figure 2. SEM images recorded for a series of $PGMA_{51}$−$PBzMA_y$ nanoparticles (where y = 200, 400, or 800) adsorbed onto PAGEO5MA brushes (~32 nm dry brush thickness) grown from planar silicon wafers. Nanoparticle adsorption experiments were conducted at 25 °C using aqueous dispersions adjusted to pH 4, 7, or 10.

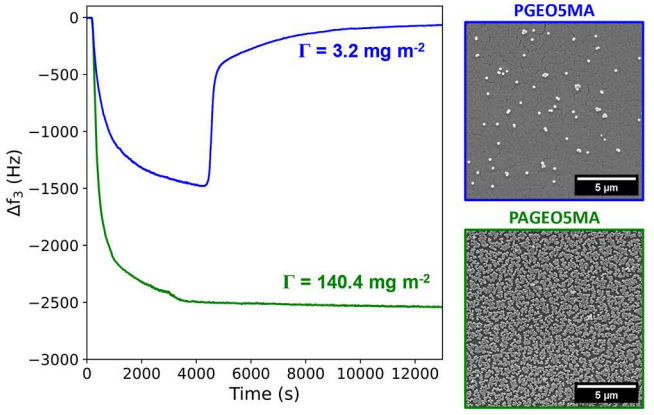

Figure 3. QCM experiments and SEM studies conducted at 25 °C for the adsorption of $PGMA_{51}$−$PBzMA_{800}$ nanoparticles onto either PAGEO5MA or PGEO5MA brushes (≈32 nm dry brush thickness) grown from either a silica QCM sensor or a planar silicon wafer (SEM). Adsorbed amounts are calculated from QCM experiments using the Sauerbrey equation.

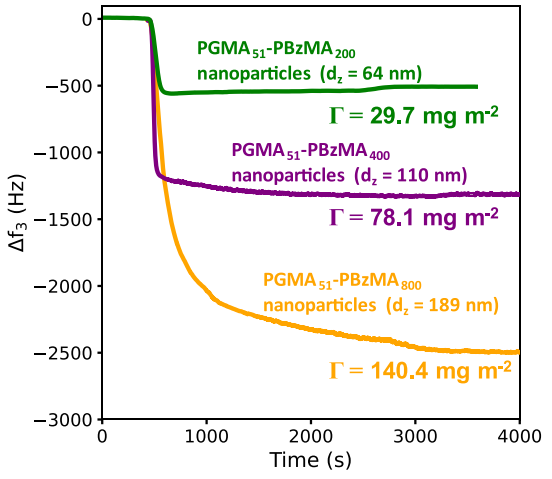

Figure 4. QCM experiments conducted at 25 °C for the adsorption of $PGMA_{51}$−$PBzMA_y$ nanoparticles [for y = 200 (upper curve), y = 400 (middle curve), or y = 800 (lower curve)] onto PAGEO5MA brushes at pH 4.

bare silicon wafer (i.e., no brush layer) was negligible (Figure S6).

QCM was also employed to quantify the adsorbed mass of the three types of nanoparticles on the PAGEO5MA brush layer (Figure 4). According to Figure 2, the mean nanoparticle surface coverage is approximately constant regardless of the particle size. However, a larger reduction in frequency was observed with increasing nanoparticle diameter. This is physically reasonable as mass scales with the cube of the nanoparticle radius, whereas surface area scales only as the square of the nanoparticle radius.

Finally, we sought to demonstrate that the adsorption of *cis*-diol-functionalized nanoparticles onto aldehyde-functional brushes really does involve chemical adsorption (i.e., acetal bond formation), rather than merely strong physical adsorption. In principle, these two modes of adsorption can be distinguished by performing temperature-dependent adsorption studies.[15,86] Thus, in the case of chemical

https://doi.org/10.1021/acs.langmuir.3c03392
Langmuir 2024, 40, 3667−3676

adsorption, the adsorbed amount should *increase* with temperature, since this favors the formation of additional acetal bonds.[87,88] In contrast, merely physical adsorption should be characterized by a *reduction* in the adsorbed amount. Accordingly, the adsorption of $PGMA_{51}$−$PBzMA_{800}$ nanoparticles onto a PAGEO5MA brush was studied by QCM from 25 to 40 °C, see Figure 5. Clearly, the adsorbed amount

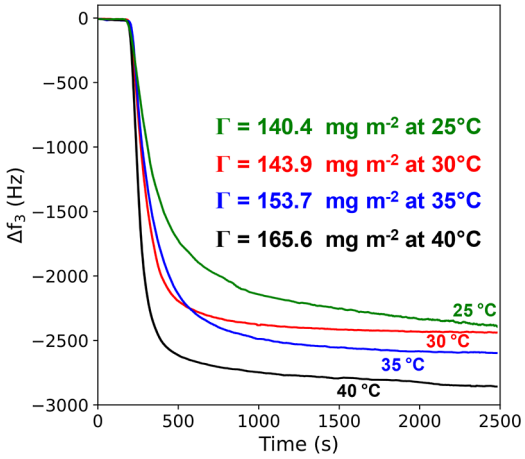

Figure 5. Temperature dependence of the adsorbed amount for $PGMA_{51}$−$PBzMA_{800}$ nanoparticles bound to a PAGEO5MA brush at pH 4 for the 25−40 °C interval as indicated by QCM studies. The adsorbed amount is arbitrarily determined after 2500 s (25 min) in each case. Greater adsorption at higher temperature provides strong evidence for chemical adsorption of the nanoparticles via acetal bond formation.

increases significantly at higher temperatures, which is consistent with the proposed formation of acetal bonds between the nanoparticles and the brush chains.

CONCLUSIONS

Three examples of sterically stabilized diblock copolymer nanoparticles bearing *cis*-diol functionality were prepared using an efficient aqueous PISA formulation. A well-defined spherical morphology was observed in each case, and the DLS z-average particle diameter was readily adjusted from 64 to 189 nm simply by varying the target DP for the core-forming poly(benzyl methacrylate) block.

In mildly acidic aqueous solution, such hydroxy-functional nanoparticles react readily with an aldehyde-functional hydrophilic brush, with QCM and SEM studies indicating relatively high adsorbed amounts of 140 mg m^{-2} and surface coverages of up to 61%, respectively. However, only minimal nanoparticle adsorption occurs in either neutral or alkaline solution, indicating that exquisite control over the extent of adsorption can be achieved via pH modulation. Finally, temperature-dependent QCM studies confirm that significantly higher adsorbed amounts are obtained at higher temperatures, which provides strong evidence for chemical adsorption via acetal bond formation. This model system provides an exemplar for the interaction of reactive sterically stabilized nanoparticles with soft substrates (e.g., hydrophilic polymer brushes).

ASSOCIATED CONTENT

Supporting Information

The Supporting Information is available free of charge at https://pubs.acs.org/doi/10.1021/acs.langmuir.3c03392.

Assigned ^{1}H NMR spectra for the $PGMA_{51}$ precursor and $PGMA_{51}$−$PBzMA_{200}$; DMF GPC data for $PGMA_{51}$, $PGMA_{51}$−$PBzMA_{200}$, $PGMA_{51}$−$PBzMA_{400}$, and $PGMA_{51}$−$PBzMA_{800}$; summary of DLS and TEM particle size data; zeta potential vs pH curves obtained for 1.0% w/w aqueous dispersions of $PGMA_{51}$−$PBzMA_{200}$, $PGMA_{51}$−$PBzMA_{400}$, and $PGMA_{51}$−$PBzMA_{800}$ nanoparticles; summary of surface coverages calculated from SEM images after nanoparticle adsorption at pH 4, 7, or 10 onto a PAGEO5MA brush; SEM images recorded after the attempted adsorption of $PGMA_{51}$−$PBzMA_{800}$ nanoparticles at pH 4, 7, or 10 onto a PGEO5MA brush; and SEM images recorded after the attempted adsorption of $PGMA_{51}$−$PBzMA_{800}$ nanoparticles at pH 4, 7, or 10 onto a planar silicon wafer (PDF)

AUTHOR INFORMATION

Corresponding Authors

Edwin C. Johnson − *Department of Chemistry, The University of Sheffield, Sheffield, South Yorkshire S3 7HF, U.K.*; orcid.org/0000-0002-0092-1008; Email: e.c.johnson@sheffield.ac.uk

Steven P. Armes − *Department of Chemistry, The University of Sheffield, Sheffield, South Yorkshire S3 7HF, U.K.*; orcid.org/0000-0002-8289-6351; Email: s.p.armes@sheffield.ac.uk

Authors

Samuel Astier − *Department of Chemistry, The University of Sheffield, Sheffield, South Yorkshire S3 7HF, U.K.*; Present Address: Normandie Univ, ENSICAEN, UNICAEN, CNRS, Laboratoire de Chimie Moléculaire et Thio-organique (LCMT) UMR 6507, 6 Bd du Maréchal Juin, 14000 Caen, France

Oleta Norvilaite − *Department of Chemistry, The University of Sheffield, Sheffield, South Yorkshire S3 7HF, U.K.*

Spyridon Varlas − *Department of Chemistry, The University of Sheffield, Sheffield, South Yorkshire S3 7HF, U.K.*; orcid.org/0000-0002-4171-7572

Emma E. Brotherton − *Department of Chemistry, The University of Sheffield, Sheffield, South Yorkshire S3 7HF, U.K.*

George Sanderson − *GEO Specialty Chemicals, Southampton, Hampshire SO45 3ZG, U.K.*

Graham J. Leggett − *Department of Chemistry, The University of Sheffield, Sheffield, South Yorkshire S3 7HF, U.K.*; orcid.org/0000-0002-4315-9076

Complete contact information is available at: https://pubs.acs.org/10.1021/acs.langmuir.3c03392

Notes

The authors declare no competing financial interest.

ACKNOWLEDGMENTS

G.J.L. and S.P.A. acknowledge an EPSRC programme grant (EP/T012455/1) for postdoctoral support of E.C.J. and S.P.A. also acknowledges an EPSRC responsive mode grant (EP/W022214/01). We thank GEO Specialty Chemicals for the synthesis of the GEO5MA monomer utilized in this study. Raffaele Battaglia and Marco Mauro at Novaetech S.r.l.

https://doi.org/10.1021/acs.langmuir.3c03392
Langmuir 2024, 40, 3667−3676

(Pompeii, Italy) are thanked for their excellent technical support regarding the QCM studies.

REFERENCES

(1) Keddie, J. L.; Meredith, P.; Jones, R. A. L.; Donald, A. M. Kinetics of film formation in acrylic latices studied with multiple-angle-of-incidence ellipsometry and environmental sem. *Macromolecules* **1995**, *28* (8), 2673−2682.
(2) Du Chesne, A.; Bojkova, A.; Gapinski, J.; Seip, D.; Fischer, P. Film formation and redispersion of waterborne latex coatings. *J. Colloid Interface Sci.* **2000**, *224* (1), 91−98.
(3) do Amaral, M.; Roos, A.; Asua, J. M.; Creton, C. Assessing the effect of latex particle size and distribution on the rheological and adhesive properties of model waterborne acrylic pressure-sensitive adhesives films. *J. Colloid Interface Sci.* **2005**, *281* (2), 325−338.
(4) Dinsmore, A. D.; Hsu, M. F.; Nikolaides, M. G.; Marquez, M.; Bausch, A. R.; Weitz, D. A. Colloidosomes: selectively permeable capsules composed of colloidal particles. *Science* **2002**, *298* (5595), 1006−1009.
(5) Binks, B. P. Particles as surfactants—similarities and differences. *Curr. Opin. Colloid Interface Sci.* **2002**, *7* (1−2), 21−41.
(6) Lobel, B. T.; Thomas, C. A.; Ireland, P. M.; Wanless, E. J.; Webber, G. B. Liquid marbles, formation and locomotion using external fields and forces. *Adv. Powder Technol.* **2021**, *32* (6), 1823−1832.
(7) Fujii, S. Liquid marble as an amphibious carrier for the controlled delivery and release of substances. *Langmuir* **2022**, *38* (42), 12757−12763.
(8) Querec, T. D.; Akondy, R. S.; Lee, E. K.; Cao, W.; Nakaya, H. I.; Teuwen, D.; Pirani, A.; Gernert, K.; Deng, J.; Marzolf, B.; Kennedy, K.; Wu, H.; Bennouna, S.; Oluoch, H.; Miller, J.; Vencio, R. Z.; Mulligan, M.; Aderem, A.; Ahmed, R.; Pulendran, B. Systems biology approach predicts immunogenicity of the yellow fever vaccine in humans. *Nat. Immunol.* **2008**, *10* (1), 116−125.
(9) Dupin, D.; Armes, S. P.; Fujii, S. Stimulus-responsive liquid marbles. *J. Am. Chem. Soc.* **2009**, *131* (15), 5386−5387.
(10) Fujii, S.; Ryan, A. J.; Armes, S. P. Long-range structural order, moiré patterns, and iridescence in latex-stabilized foams. *J. Am. Chem. Soc.* **2006**, *128* (24), 7882−7886.
(11) Brewer, S. H.; Glomm, W. R.; Johnson, M. C.; Knag, M. K.; Franzen, S. Probing BSA binding to citrate-coated gold nanoparticles and surfaces. *Langmuir* **2005**, *21* (20), 9303−9307.
(12) Fatisson, J.; Domingos, R. F.; Wilkinson, K. J.; Tufenkji, N. Deposition of tio $_2$ nanoparticles onto silica measured using a quartz crystal microbalance with dissipation monitoring. *Langmuir* **2009**, *25* (11), 6062−6069.
(13) Engström, J.; Reid, M. S.; Brotherton, E. E.; Malmström, E.; Armes, S. P.; Hatton, F. L. Investigating the adsorption of anisotropic diblock copolymer worms onto planar silica and nanocellulose surfaces using a quartz crystal microbalance. *Polym. Chem.* **2021**, *12* (42), 6088−6100.
(14) Brotherton, E. E.; Josland, D.; György, C.; Johnson, E. C.; Chan, D. H. H.; Smallridge, M. J.; Armes, S. P. Histidine-functionalized diblock copolymer nanoparticles exhibit enhanced adsorption onto planar stainless steel. *Macromol. Rapid Commun.* **2023**, *44*, 2200903.
(15) György, C.; Kirkman, P. M.; Neal, T. J.; Chan, D. H. H.; Williams, M.; Smith, T.; Growney, D. J.; Armes, S. P. Enhanced adsorption of epoxy-functional nanoparticles onto stainless steel significantly reduces friction in tribological studies. *Angew. Chem., Int. Ed.* **2023**, *62* (10), No. e202218397.
(16) Xu, D.; Hodges, C.; Ding, Y.; Biggs, S.; Brooker, A.; York, D. Adsorption kinetics of laponite and Ludox silica nanoparticles onto a deposited poly(diallyldimethylammonium chloride) layer measured by a quartz crystal microbalance and optical reflectometry. *Langmuir* **2010**, *26* (23), 18105−18112.
(17) Uludag, Y.; Tothill, I. E. Cancer biomarker detection in serum samples using surface plasmon resonance and quartz crystal microbalance sensors with nanoparticle signal amplification. *Anal. Chem.* **2012**, *84* (14), 5898−5904.
(18) Mao, X.; Yang, L.; Su, X. L.; Li, Y. A nanoparticle amplification based quartz crystal microbalance dna sensor for detection of Escherichia coli o157:h7. *Biosens. Bioelectron.* **2006**, *21* (7), 1178−1185.
(19) Sener, G.; Ozgur, E.; Yılmaz, E.; Uzun, L.; Say, R.; Denizli, A. Quartz crystal microbalance based nanosensor for lysozyme detection with lysozyme imprinted nanoparticles. *Biosens. Bioelectron.* **2010**, *26* (2), 815−821.
(20) Suthar, J.; Parsons, E. S.; Hoogenboom, B. W.; Williams, G. R.; Guldin, S. Acoustic immunosensing of exosomes using a quartz crystal microbalance with dissipation monitoring. *Anal. Chem.* **2020**, *92* (5), 4082−4093.
(21) Sakai, K.; Vamvakaki, M.; Smith, E. G.; Wanless, E. J.; Armes, S. P.; Biggs, S. Adsorption characteristics of zwitterionic diblock copolymers at the silica/aqueous solution interface. *J. Colloid Interface Sci.* **2008**, *317* (2), 383−394.
(22) Sakai, K.; Webber, G. B.; Vo, C.-D.; Wanless, E. J.; Vamvakaki, M.; Bütün, V.; Armes, S. P.; Biggs, S. Characterization of layer-by-layer self-assembled multilayer films of diblock copolymer micelles. *Langmuir* **2008**, *24* (1), 116−123.
(23) Sakai, K.; Smith, E. G.; Webber, G. B.; Baker, M.; Wanless, E. J.; Bütün, V.; Armes, S. P.; Biggs, S. PH-responsive behavior of selectively quaternized diblock copolymers adsorbed at the silica/aqueous solution interface. *J. Colloid Interface Sci.* **2007**, *314* (2), 381−388.
(24) Sakai, K.; Smith, E. G.; Webber, G. B.; Wanless, E. J.; Bütün, V.; Armes, S. P.; Biggs, S. Effects of copolymer concentration and chain length on the ph-responsive behavior of diblock copolymer micellar films. *J. Colloid Interface Sci.* **2006**, *303* (2), 372−379.
(25) Sakai, K.; Smith, E. G.; Webber, G. B.; Schatz, C.; Wanless, E. J.; Bütün, V.; Armes, S. P.; Biggs, S. PH-responsive diblock copolymer micelles at the silica/aqueous solution interface: adsorption kinetics and equilibrium studies. *J. Phys. Chem. B* **2006**, *110* (30), 14744−14753.
(26) Sakai, K.; Smith, E. G.; Webber, G. B.; Baker, M.; Wanless, E. J.; Bütün, V.; Armes, S. P.; Biggs, S. Characterizing the ph-responsive behavior of thin films of diblock copolymer micelles at the silica/aqueous solution interface. *Langmuir* **2006**, *22* (20), 8435−8442.
(27) Olsson, A. L. J.; Quevedo, I. R.; He, D.; Basnet, M.; Tufenkji, N. Using the quartz crystal microbalance with dissipation monitoring to evaluate the size of nanoparticles deposited on surfaces. *ACS Nano* **2013**, *7* (9), 7833−7843.
(28) Grunewald, C.; Schmudde, M.; Noufele, C. N.; Graf, C.; Risse, T. Ordered structures of functionalized silica nanoparticles on gold surfaces: correlation of quartz crystal microbalance with structural characterization. *Anal. Chem.* **2015**, *87* (20), 10642−10649.
(29) Yousefi, N.; Tufenkji, N. Probing the interaction between nanoparticles and lipid membranes by quartz crystal microbalance with dissipation monitoring. *Front. Chem.* **2016**, *4*, 236509.
(30) D'Agosto, F.; Rieger, J.; Lansalot, M. RAFT-mediated polymerization-induced self-assembly. *Angew. Chem., Int. Ed.* **2020**, *59* (22), 8368−8392.
(31) Biais, P.; Colombani, O.; Bouteiller, L.; Stoffelbach, F.; Rieger, J. Unravelling the formation of bab block copolymer assemblies during pisa in water. *Polym. Chem.* **2020**, *11* (28), 4568−4578.
(32) Mellot, G.; Beaunier, P.; Guigner, J. M.; Bouteiller, L.; Rieger, J.; Stoffelbach, F. Beyond simple ab diblock copolymers: application of bifunctional and trifunctional raft agents to pisa in water. *Macromol. Rapid Commun.* **2019**, *40* (2), 1800315.
(33) Ebeling, B.; Belal, K.; Stoffelbach, F.; Woisel, P.; Lansalot, M.; D'Agosto, F. Polymer nanospheres with hydrophobic surface groups as supramolecular building blocks produced by aqueous pisa. *Macromol. Rapid Commun.* **2019**, *40* (2), 1800455.
(34) Wang, X.; An, Z. New insights into raft dispersion polymerization-induced self-assembly: from monomer library, morphological control, and stability to driving forces. *Macromol. Rapid Commun.* **2019**, *40* (2), 1800325.

https://doi.org/10.1021/acs.langmuir.3c03392
Langmuir 2024, 40, 3667−3676

(35) Zhang, W. J.; Hong, C. Y.; Pan, C. Y. Polymerization-induced self-assembly of functionalized block copolymer nanoparticles and their application in drug delivery. *Macromol. Rapid Commun.* **2019**, *40* (2), 1800279.
(36) Penfold, N. J. W.; Yeow, J.; Boyer, C.; Armes, S. P. Emerging trends in polymerization-induced self-assembly. *ACS Macro Lett.* **2019**, *8* (8), 1029−1054.
(37) Canning, S. L.; Smith, G. N.; Armes, S. P. A critical appraisal of raft-mediated polymerization-induced self-assembly. *Macromolecules* **2016**, *49* (6), 1985−2001.
(38) György, C.; Armes, S. P. Recent advances in polymerization-induced self-assembly (PISA) syntheses in non-polar media. *Angew. Chem., Int. Ed.* **2023**, *62*, No. e202308372.
(39) Yamanaka, R.; Sugawara-Narutaki, A.; Takahashi, R. In situ monitoring of polymerization-induced self-assembly and gelation during the synthesis of triblock copolymers via time-resolved small-angle x-ray scattering and rheology. *Macromolecules* **2023**, *56* (11), 4354−4361.
(40) Takahashi, R.; Miwa, S.; Sobotta, F. H.; Lee, J. H.; Fujii, S.; Ohta, N.; Brendel, J. C.; Sakurai, K. Unraveling the kinetics of the structural development during polymerization-induced self-assembly: decoupling the polymerization and the micelle structure. *Polym. Chem.* **2020**, *11* (8), 1514−1524.
(41) Derry, M. J.; Fielding, L. A.; Armes, S. P. Polymerization-induced self-assembly of block copolymer nanoparticles via raft non-aqueous dispersion polymerization. *Prog. Polym. Sci.* **2016**, *52*, 1−18.
(42) Zhang, W.; D'Agosto, F.; Dugas, P.-Y.; Rieger, J.; Charleux, B. RAFT-mediated one-pot aqueous emulsion polymerization of methyl methacrylate in presence of poly[methacrylic acid-co-poly(ethylene oxide) methacrylate] trithiocarbonate macromolecular chain transfer agent. *Polymer* **2013**, *54* (8), 2011−2019.
(43) Shahrokhinia, A.; Scanga, R. A.; Biswas, P.; Reuther, J. F. PhotoATRP-induced self-assembly (PhotoATR-PISA) enables simplified synthesis of responsive polymer nanoparticles in one-pot. *Macromolecules* **2021**, *54* (3), 1441−1451.
(44) Karagoz, B.; Esser, L.; Duong, H. T.; Basuki, J. S.; Boyer, C.; Davis, T. P. Polymerization-induced self-assembly (pisa)—control over the morphology of nanoparticles for drug delivery applications. *Polym. Chem.* **2014**, *5* (2), 350−355.
(45) Charleux, B.; Delaittre, G.; Rieger, J.; D'Agosto, F. Polymerization-induced self-assembly: from soluble macromolecules to block copolymer nano-objects in one step. *Macromolecules* **2012**, *45* (17), 6753−6765.
(46) Parker, B. R.; Derry, M. J.; Ning, Y.; Armes, S. P. Exploring the upper size limit for sterically stabilized diblock copolymer nanoparticles prepared by polymerization-induced self-assembly in non-polar media. *Langmuir* **2020**, *36* (14), 3730−3736.
(47) Jones, E. R.; Mykhaylyk, O. O.; Semsarilar, M.; Boerakker, M.; Wyman, P.; Armes, S. P. How do spherical diblock copolymer nanoparticles grow during raft alcoholic dispersion polymerization? *Macromolecules* **2016**, *49* (1), 172−181.
(48) Truong, N. P.; Dussert, M. V.; Whittaker, M. R.; Quinn, J. F.; Davis, T. P. Rapid synthesis of ultrahigh molecular weight and low polydispersity polystyrene diblock copolymers by raft-mediated emulsion polymerization. *Polym. Chem.* **2015**, *6* (20), 3865−3874.
(49) Chaduc, I.; Girod, M.; Antoine, R.; Charleux, B.; D'Agosto, F.; Lansalot, M. Batch emulsion polymerization mediated by poly(methacrylic acid) macroraft agents: one-pot synthesis of self-stabilized particles. *Macromolecules* **2012**, *45* (15), 5881−5893.
(50) Rieger, J.; Osterwinter, G.; Bui, C.; Stoffelbach, F.; Charleux, B. Surfactant-free controlled/living radical emulsion (co)polymerization of *n* -butyl acrylate and methyl methacrylate via raft using amphiphilic poly(ethylene oxide)-based trithiocarbonate chain transfer agents. *Macromolecules* **2009**, *42* (15), 5518−5525.
(51) Rieger, J.; Stoffelbach, F.; Bui, C.; Alaimo, D.; Jérôme, C.; Charleux, B. Amphiphilic poly(ethylene oxide) macromolecular raft agent as a stabilizer and control agent in ab initio batch emulsion polymerization. *Macromolecules* **2008**, *41* (12), 4065−4068.
(52) Cunningham, V. J.; Alswieleh, A. M.; Thompson, K. L.; Williams, M.; Leggett, G. J.; Armes, S. P.; Musa, O. M. Poly(glycerol monomethacrylate)-poly(benzyl methacrylate) diblock copolymer nanoparticles via raft emulsion polymerization: synthesis, characterization, and interfacial activity. *Macromolecules* **2014**, *47* (16), 5613−5623.
(53) North, S. M.; Jones, E. R.; Smith, G. N.; Mykhaylyk, O. O.; Annable, T.; Armes, S. P. Adsorption of small cationic nanoparticles onto large anionic particles from aqueous solution: a model system for understanding pigment dispersion and the problem of effective particle density. *Langmuir* **2017**, *33* (5), 1275−1284.
(54) Akpinar, B.; Fielding, L. A.; Cunningham, V. J.; Ning, Y.; Mykhaylyk, O. O.; Fowler, P. W.; Armes, S. P. Determining the effective density and stabilizer layer thickness of sterically stabilized nanoparticles. *Macromolecules* **2016**, *49* (14), 5160−5171.
(55) Ning, Y.; Fielding, L. A.; Doncom, K. E. B.; Penfold, N. J. W.; Kulak, A. N.; Matsuoka, H.; Armes, S. P. Incorporating diblock copolymer nanoparticles into calcite crystals: do anionic carboxylate groups alone ensure efficient occlusion? *ACS Macro Lett.* **2016**, *5* (3), 311−315.
(56) Ning, Y.; Armes, S. P.; Li, D. Polymer-inorganic crystalline nanocomposite materials via nanoparticle occlusion. *Macromol. Rapid Commun.* **2022**, *43* (14), 2100793.
(57) Chan, D. H. H.; Deane, O. J.; Kynaston, E. L.; Lindsay, C.; Taylor, P.; Armes, S. P. Sterically stabilized diblock copolymer nanoparticles enable convenient preparation of suspension concentrates comprising various agrochemical actives. *Langmuir* **2022**, *38* (9), 2885−2894.
(58) Chan, D. H.; Millet, A.; Fisher, C. R.; Price, M. C.; Burchell, M. J.; Armes, S. P. Synthesis and characterization of polypyrrole-coated anthracene microparticles: a new synthetic mimic for polyaromatic hydrocarbon-based cosmic dust. *ACS Appl. Mater. Interfaces* **2021**, *13* (2), 3175−3185.
(59) Johnson, E. C.; Varlas, S.; Norvilaite, O.; Neal, T. J.; Brotherton, E. E.; Sanderson, G.; Leggett, G. J.; Armes, S. P. Adsorption of aldehyde-functional diblock copolymer spheres onto surface-grafted polymer brushes via dynamic covalent chemistry enables friction modification. *Chem. Mater.* **2023**, *35* (15), 6109−6122.
(60) Reviakine, I.; Johannsmann, D.; Richter, R. P. Hearing what you cannot see and visualizing what you hear: interpreting quartz crystal microbalance data from solvated interfaces. *Anal. Chem.* **2011**, *83* (23), 8838−8848.
(61) Cho, N.-J.; Frank, C. W.; Kasemo, B.; Höök, F. Quartz crystal microbalance with dissipation monitoring of supported lipid bilayers on various substrates. *Nat. Protoc.* **2010**, *5* (6), 1096−1106.
(62) Brotherton, E. E.; Johnson, E. C.; Smallridge, M. J.; Hammond, D. B.; Leggett, G. J.; Armes, S. P. Hydrophilic aldehyde-functional polymer brushes: synthesis, characterization, and potential bioapplications. *Macromolecules* **2023**, *56* (5), 2070−2080.
(63) Derry, M. J.; Fielding, L. A.; Armes, S. P. Industrially-relevant polymerization-induced self-assembly formulations in non-polar solvents: raft dispersion polymerization of benzyl methacrylate. *Polym. Chem.* **2015**, *6* (16), 3054−3062.
(64) Ning, Y.; Whitaker, D. J.; Mable, C. J.; Derry, M. J.; Penfold, N. J. W.; Kulak, A. N.; Green, D. C.; Meldrum, F. C.; Armes, S. P. Anionic block copolymer vesicles act as trojan horses to enable efficient occlusion of guest species into host calcite crystals. *Chem. Sci.* **2018**, *9* (44), 8396−8401.
(65) Zhang, Y.; Wang, Z.; Matyjaszewski, K.; Pietrasik, J. Evolution of morphology of POEGMA-b-PBzMA nano-objects formed by pisa. *Macromol. Rapid Commun.* **2019**, *40* (2), 1800331.
(66) Cunningham, V. J.; Ning, Y.; Armes, S. P.; Musa, O. M. Poly(n-2-(methacryloyloxy)ethyl pyrrolidone)-poly(benzyl methacrylate) diblock copolymer nano-objects via raft alcoholic dispersion polymerisation in ethanol. *Polymer* **2016**, *106*, 189−199.
(67) Jones, E. R.; Semsarilar, M.; Blanazs, A.; Armes, S. P. Efficient synthesis of amine-functional diblock copolymer nanoparticles via raft

https://doi.org/10.1021/acs.langmuir.3c03392
Langmuir 2024, 40, 3667−3676

dispersion polymerization of benzyl methacrylate in alcoholic media. *Macromolecules* **2012**, *45* (12), 5091−5098.
(68) Moad, G.; Rizzardo, E.; Thang, S. H. RAFT polymerization and some of its applications. *Chem. Asian J.* **2013**, *8* (8), 1634−1644.
(69) Edmondson, S.; Huck, W. T. S. Controlled growth and subsequent chemical modification of poly(glycidyl methacrylate) brushes on silicon wafers. *J. Mater. Chem.* **2004**, *14* (4), 730−734.
(70) Yang, W. J.; Neoh, K.-G.; Kang, E.-T.; Teo, S. L.-M.; Rittschof, D. Polymer brush coatings for combating marine biofouling. *Prog. Polym. Sci.* **2014**, *39* (5), 1017−1042.
(71) Ye, Q.; He, B.; Zhang, Y.; Zhang, J.; Liu, S.; Zhou, F. Grafting robust thick zwitterionic polymer brushes via subsurface-initiated ring-opening metathesis polymerization for antimicrobial and anti-biofouling. *ACS Appl. Mater. Interfaces* **2019**, *11* (42), 39171−39178.
(72) Halperin, A.; Kröger, M.; Zhulina, E. B. Colloid-brush interactions: the effect of solvent quality. *Macromolecules* **2011**, *44* (9), 3622−3638.
(73) Laktionov, M. Y.; Shavykin, O. V.; Leermakers, F. A. M.; Zhulina, E. B.; Borisov, O. V. Colloidal particles interacting with a polymer brush: a self-consistent field theory. *Phys. Chem. Chem. Phys.* **2022**, *24* (14), 8463−8476.
(74) Zhang, Q.; Xiang, X. Adsorption of a spherical nanoparticle in polymer brushes: Brownian dynamics investigation. *Physica A* **2013**, *392* (18), 3857−3862.
(75) Lian, Z.; Qi, S. Size effect of the end-attached particle on the adsorption-responsive polymer switches. *Macromolecules* **2022**, *55* (18), 8162−8175.
(76) de Beer, S.; Mensink, L. I. S.; Kieviet, B. D. Geometry-dependent insertion forces on particles in swollen polymer brushes. *Macromolecules* **2016**, *49* (3), 1070−1078.
(77) Showler, A. J.; Darley, P. A. Condensation products of glycerol with aldehydes and ketones. 2-substituted m-dioxan-5-ols and 1,3-dioxolane-4-methanols. *Chem. Rev.* **1967**, *67* (4), 427−440.
(78) Fife, T. H.; Natarajan, R. General acid catalyzed acetal hydrolysis. the hydrolysis of acetals and ketals of cis- and trans-1,2-cyclohexanediol. changes in rate-determining step and mechanism as a function of ph. *J. Am. Chem. Soc.* **1986**, *108* (25), 8050−8056.
(79) Easley, A. D.; Ma, T.; Eneh, C. I.; Yun, J.; Thakur, R. M.; Lutkenhaus, J. L. A practical guide to quartz crystal microbalance with dissipation monitoring of thin polymer films. *J. Polym. Sci.* **2022**, *60* (7), 1090−1107.
(80) Johnson, E. C.; Murdoch, T. J.; Gresham, I. J.; Humphreys, B. A.; Prescott, S. W.; Nelson, A.; Webber, G. B.; Wanless, E. J. Temperature dependent specific ion effects in mixed salt environments on a thermoresponsive poly(oligoethylene glycol methacrylate) brush. *Phys. Chem. Chem. Phys.* **2019**, *21* (8), 4650−4662.
(81) Gresham, I. J.; Willott, J. D.; Johnson, E. C.; Li, P.; Webber, G. B.; Wanless, E. J.; Nelson, A. R. J.; Prescott, S. W. Effect of surfactants on the thermoresponse of PNIPAM investigated in the brush geometry. *J. Colloid Interface Sci.* **2023**, *631*, 260−271.
(82) Gresham, I. J.; Johnson, E. C.; Robertson, H.; Willott, J. D.; Webber, G. B.; Wanless, E. J.; Nelson, A. R. J.; Prescott, S. W. Comparing polymer-surfactant complexes to polyelectrolytes. *J. Colloid Interface Sci.* **2024**, *655*, 262−272.
(83) Hunter, S. J.; Abu Elella, M. H.; Johnson, E. C.; Taramova, L.; Brotherton, E. E.; Armes, S. P.; Khutoryanskiy, V. V.; Smallridge, M. J. Mucoadhesive pickering nanoemulsions via dynamic covalent chemistry. *J. Colloid Interface Sci.* **2023**, *651*, 334−345.
(84) Xiao, X.; Chen, C.; Zhang, Y.; Kong, H.; An, R.; Li, S.; Liu, W.; Ji, Q. Chiral recognition on bare gold surfaces by quartz crystal microbalance. *Angew. Chem., Int. Ed.* **2021**, *60* (47), 25028−25033.
(85) Cui, M.; Duan, Y.; Ma, Y.; Al-Shwafy, K. W. A.; Liu, Y.; Zhao, X.; Huang, R.; Qi, W.; He, Z.; Su, R. Real-time QCM-D monitoring of the adsorption-desorption of expansion on lignin. *Langmuir* **2020**, *36* (16), 4503−4510.
(86) Halsey, G. Physical adsorption on non-uniform surfaces. *J. Chem. Phys.* **1948**, *16* (10), 931−937.
(87) Rettner, C. T.; Auerbach, D. J.; Tully, J. C.; Kleyn, A. W. Chemical dynamics at the gas-surface interface. *J. Phys. Chem.* **1996**, *100* (31), 13021−13033.
(88) Shimizu, S.; Matubayasi, N. Temperature dependence of sorption. *Langmuir* **2021**, *37* (37), 11008−11017.

https://doi.org/10.1021/acs.langmuir.3c03392
Langmuir 2024, 40, 3667−3676